RESEARCH

Design of Graphene-Based Tunable Plasmonic Antenna for Multiband Terahertz Application Systems

Sattar Othman Hasan[1,2] · Saman Khabbat Ezzulddin[2] · Hersh Ahmed Khizir[2] · Muhamad Abdullah Hamad[1] · Bushra Adnan Rahman[1]

Abstract

This article presents a systematic technique for designing a novel multiband plasmonic antenna based on graphene with a silicon nitride (SiO_3N_4) dielectric substrate in the terahertz band frequencies. Higher conductivity values are found in the 1–5 THz ranges when the graphene conductivity values are measured at these band frequencies. Based on this, graphene chemical potential (μ_c) values between 0.0 and 1.0 eV are implemented to derive the fundamental antenna parameters. According to the simulated results, the proposed antenna operates at dual-band frequencies when μ_c is less than 0.3 eV and at triple-band frequencies when it is greater than that. Furthermore, for terahertz applications, the chemical potential value of 0.5 eV appears more reliable as the suggested antenna is operated at a tri-band frequency of 0.855, 3.760, and 4.650 THz with a gain of 3.06, 7.65, and 7.53 dB and fraction bandwidth of 32.4%, 5.21%, and 4.24%, respectively. Furthermore, the advancement of the current work was evident when comparing the obtained results with those previously achieved by other researchers, particularly in terms of antenna size, gain, and bandwidth values. Finally, it can be concluded that the recommended antenna offers good frequency tunable features and is suitable for high-speed indoor wireless applications.

Keywords Plasmonic antenna · Graphene · Chemical potential · Microstrip antenna · Terahertz

Introduction

THz radiation has the advantages of numerous range of applications in the field of recent surveillance communication systems due to non-ionizing properties as well as large transmission capability [1]. In the electromagnetic (EM) spectrum with THz, frequency is placed between the microwave (mm) and infrared (IR) bands that possesses a particular property of the microwave and light waves. Hence, the terahertz (EM) waves are allowed to begin from both the electronic and photonic device [2, 3]. With the quick growth of terahertz detectors and sources, THz band has gained more attention in the field of wireless communication systems [4]. An important component of communication technology is the antenna that is used to transmit and receive information in the form of electromagnetic (EM) wave. The antennas used in the THz region should be capable of providing high gain, wide bandwidth (BW), compact, and low cost. This leads to make the microstrip patch antennas as a suitable choice for these applications [5, 6].

Additionally, the terahertz (THz) technology needs small size of the communication and electronic devices with enhancing the data speed. The nano-antennas are advance designed using good conductor materials like copper, silver, and gold, but these conductors in nano-antenna operate at THz frequency with very high energy losses and are not easy to tuning it for resonance frequency (f_r) control [7]. To reduce these limitations, researchers are drawn towards the use of novel materials such as graphene as an alternative to aforementioned metals [8, 9].

Graphene is one layer of carbon atoms and formed in a honeycomb lattice that provides good optical characteristics that lead it to be suitable for plasmonic applications [7, 10]. Beyond that, graphene is currently popular with the interest of the research field because of its new electrical, mechanical, chemical, optical, and thermal properties [11–13]. With respect to its special properties, graphene offers wide possible

✉ Saman Khabbat Ezzulddin
  saman.ezzlddin@su.edu.krd

1 Department of Physics, College of Education, Salahaddin University-Erbil, Erbil, Iraq

2 Department of Physics, College of Science, Salahaddin University-Erbil, Erbil, Iraq

uses in a variety of fields, such as transistors with ultra-high speed, antennas [14, 15], transparent solar cells [16], waveguides [17], demultiplexers [18, 19], resonators [20], absorbers [21, 22], filters [23], and modulator [24, 25]. Currently, several graphene-based antennas have been recommended involving the leaky-wave [26], Yagi-Uda [14, 27], reconfigurable [28–30], and reflect array [31] antennas that display widespread capabilities in the THz band [32, 33].

When graphene material is integrated into antenna systems, it displays improvement in the radiation performance compared to the typical conventional antennas at very high frequencies. This is because graphene has a good conductivity and its chemical potential (μ_c) can be changed via an external electrostatic direct current (DC) or by doping during manufacturing process [34]. Besides, the relationship between momentum and energy of electrons in graphene is linear rather than quadratic through a variety of energies and this allows extremely high carrier mobility to be obtained at room temperature [35]. These graphene extraordinary properties allow it to be very interesting to promote surface plasma polariton (SPP) mode, especially in the THz frequency range, as its resonance plasma frequency is exactly located in this band [35]. On the other hand, the graphene plasmonic behavior can be employed as a radiating patch or an artificial magnetic conductor (AMC) in miniaturization process for the design of antennas [36].

In this investigation, a novel plasmonic nano-antenna based on graphene is proposed and designed on the silicon nitride (SiO_3N_4) dielectric substrate using coupled gap feeding techniques operating at 0 to 5 THz. In the first step, the graphene surface conductivity (σ_g) is calculated in the range frequency of 1 to 10 THz with various chemical potential (μ_c) values. After that, the performance of the simulated antenna is computed under the impact change of graphene chemical potential. Finally, the chemical potential values, which maintain the dual and tri-band frequency operation of the various vibration modes, are specified. Also, their impacts on the overall suggested antenna parameters are determined.

The continuing section of the present work is arranged as follows: In the "Material and Simulation Technique" section, the numerical model for computing the electric conductivity of graphene and geometry of the proposed plasmonic antenna are provided in detail. The results and dissection of the proposed antenna parameters at various operational modes are described in the "Results and Discussions" section. The main conclusions are summarized in the "Conclusion" section.

Material and Simulation Technique

The graphene-based plasmonic antenna is designed and simulated using CST software techniques. In this article, a graphene radiation patch is built up on a dielectric substrate whose bias voltage (V_g) is connected between a single layer

of graphene and antenna substrate that enhances the chemical potential (μ_c) and this in turn leads to varying graphene conductivity (σ_g).

Graphene Properties

In this section, the variation of graphene electric conductivity as a function of μ_c is studied. As indicated by [37], the graphene conductivity is complex and consists of intra-band (σ_{intra}) and inter-band (σ_{inter}) parts. Furthermore, graphene conductivity (σ_g) is dependent on the frequency which is described by Kubo's formula and it is approximately expressed as [38]

$$\sigma_g(\omega, \mu_c, s, T) = \sigma_{intra}(\omega, \mu_c, s, T) + \sigma_{inter}(\omega, \mu_c, s, T) \quad (1)$$

The conductivity of graphene due to intra-band (σ_{intra}) and inter-band (σ_{inter}) can be expressed, respectively, as given by [39, 40]

$$\sigma_{intra}(\omega, \mu_c, s, T) = -j\frac{e^2 k_B T}{\pi \hbar^2(\omega - 2j\Gamma)}\left[\frac{\mu_c}{k_B T} 2\ln\left(e^{\frac{\mu_c}{k_B T}} + 1)\right)\right] \quad (2)$$

$$\sigma_{inter}(\omega, \mu_c, s, T) = -j\frac{e^2}{4\pi\hbar}\ln\left(\frac{2|\mu_c| - (\omega - 2j\Gamma)\hbar}{2|\mu_c| + (\omega - 2j\Gamma)\hbar}\right) \quad (3)$$

where ω is the angular frequency, T is the temperature, e is the charge of the electron, μ_c is the chemical potential, k_B is Boltzmann's constant, $\hbar$ is reduced Planck's constant, and Γ is a scattering rate. However, in the range of THz frequencies, the term of inter-band has little impact on the total surface conductivity of graphene (σ_g), and hence, the intra-band conductivity term will control the value of total surface conductivity (σ_g) [41, 42].

The numerical expression of Kubo formula, as mentioned in Eqs. (2) and (3), is handled to analyze the behavior conductivity of graphene in the terahertz (THz) band frequencies using various chemical potential values. The obtained results of the real component and imaginary component of the graphene surface conductivities are displayed in Fig. 1a and b, respectively. This figure displays that the conductivity of graphene is related to the chemical potential (μ_c) and it is obviously seen that $\sigma_{real} \geq 0$ while $\sigma_{imag} \leq 0$ in the range frequency of 1 to 10 THz. It is also observed that the values of the imaginary component are greater in comparison to the values of the real component. Besides, in the frequency ranges 1–4 THz band, this figure indicates that the graphene conductivity is high compared to the other considered frequency ranges and it might be regarded as a good choice for some antenna design considerations.

Therefore, the graphene conductivities can be controlled through the applied μ_c. Since graphene conductivity values
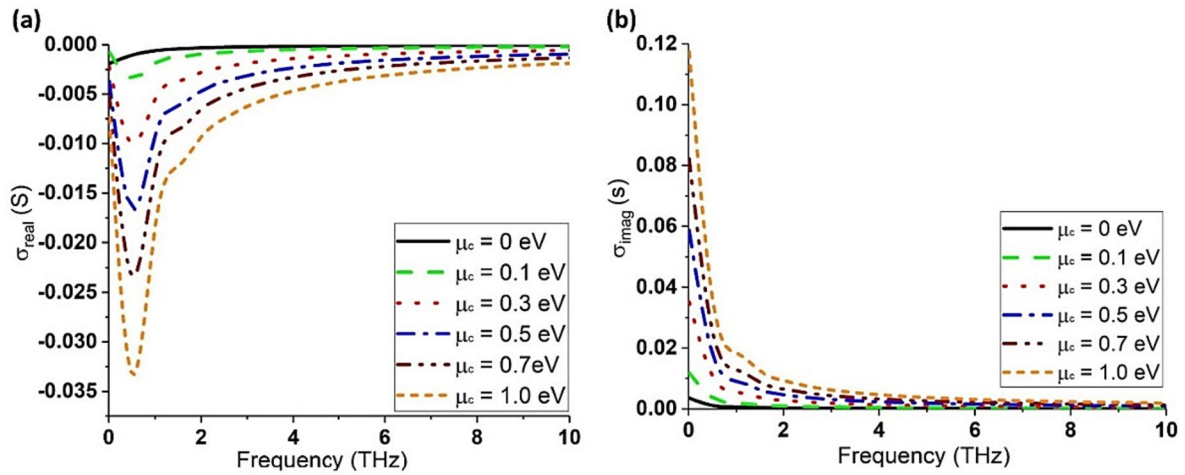
Fig. 1 Variation surface conductivity of graphene dependent on frequency with various values of μ_c using the Kubo model **a** real and **b** imaginary terms

are high relative to high values (μ_c) due to having a greater carrier density and this makes the graphene patch material to support (SPPs), which will be used to confine the incident EM wave. Moreover, the graphene material properties in terms of thermal, electrical, optical, and mechanical characteristics are displayed in Table 1.

Plasmonic Antenna Geometry

The microstrip antenna in simple form consists of dielectric substrate confinement between two parallel conductors [44]. In this work, a rectangular graphene radiation patch is placed at the upper part of the dielectric substrate of silicon nitride (SiO_3N_4). The opposed side of the antenna substrate is made up of graphene with the same dimensions of the substrate which is used like antenna ground plane as illustrated in Fig. 2. The thickness of the ground plane and the patch is considered to be the same and equal to 0.345 nm.

Table 1 Thermal, electrical, optical, and mechanical characteristics of graphene material [43]

Properties		Value	Unit
Thermal and electrical	Electronic mobility	~ 2×10^5	m²/Vs
	Band gap	0	–
	Current density	~ 10^9	A/cm
	Thermal conductivity	~ 5000	W/mK
	Fermi velocity	~ 10^6	m/s
Optical	Transparency	~ 97.70%	–
Mechanical	Tensile strength	~ 1	TPa
	Elastic limit	~ 20%	–
	Thickness	0.345	Nm
	Surface area	2360	m²/gm
	Breaking strength	42	N/m

As the bias voltage (V_g) is put into the graphene patch, the electrons inside the patch are oscillating around their equilibrium position at THz range frequencies and this phenomenon is called SPP [45, 46]. The dispersion relation of the SPP wave vector (k_{SPP}) or the transverse magnetic (TM) mode of the graphene sheet is evaluated in free space using the relation given by [47] as

$$k_{SPP} = k_\circ \sqrt{1 - \left(\frac{2}{\eta_{eff}\sigma_g} \right)^2} \approx \frac{\hbar\omega^2}{2\alpha\mu_c c} \tag{4}$$

$$\eta_{eff} = \sqrt{1 - \frac{4\mu_\circ}{\varepsilon_\circ (\sigma_g)^2}} \approx \frac{\lambda}{\lambda_{SPP}} \tag{5}$$

where λ_{SPP}, λ_0, α, k_0, and η_{eff} are, respectively, operational surface plasmonic polariton wavelength, free space wavelength, attenuation constant, wave vector, and effective intrinsic impedance of graphene material. Besides, the width (W_p) and length (L_p) of the simulated plasmonic antenna are determined through the formula expressions presented by [48] as

$$W_p = \frac{(2M + 1)}{\sqrt{\varepsilon_r}} \times \frac{\lambda_\circ}{2} \tag{6}$$

$$L_p = \frac{(2N + 1)}{\sqrt{\varepsilon_{eff}}} \times \left(\frac{\lambda_{SPP}}{2} \right) - 2\Delta L \tag{7}$$

where M and N are positive integer numbers; ε_r and ε_{eff} are relative and effective permittivity of the dielectric material, respectively; ΔL is the radiation patch length expansion as a result of the creation of fringing fields. Moreover, the width (W_f) of the microstrip line feed is determined from
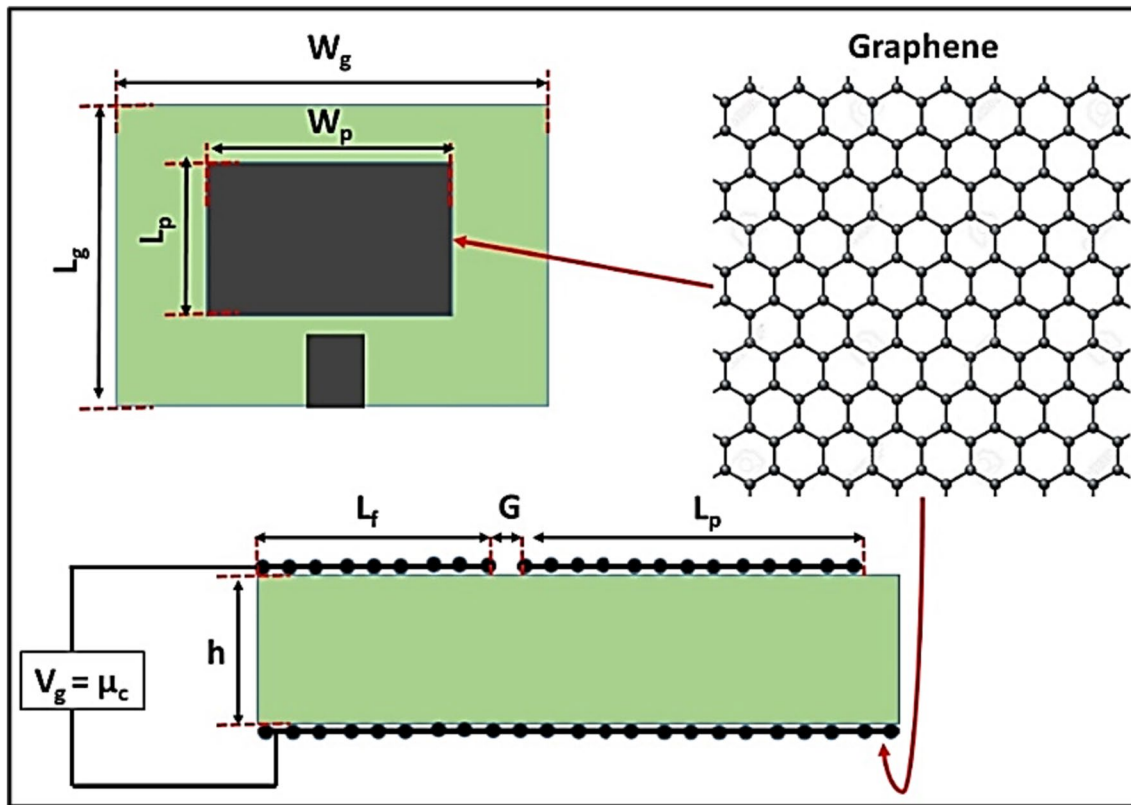
Fig. 2 Top and cross-sectional view of the graphene-based plasmonic microstrip antenna

the mathematical relation of the input antenna impedance (Z_a) given by [48] as

$$W_f = \frac{11.96\lambda_o}{Z_a} \tag{8}$$

It is worth mentioning that Z_a should be matched to characteristic impedance with the line feeding (L_f). Hence, the antenna ground and substrate dimensions are determined by using the expression given by [48] as

$$L_s = L_g = L_p + 2L_f \tag{9}$$

$$W_s = W_g = W_p + 2L_f \tag{10}$$

where L_g, W_g, L_s, and W_s are the length and width of antenna ground plane substrate material, respectively. According to

the above equations, the dimensions of the proposed antennas computed are summarized in Table 2.

At the same time, the selection of appropriate chemical potential (μ_c) values for graphene (μ_c) may significantly affect the impedance characteristics of the antenna and, therefore, the antenna resonating frequency. Furthermore, the chemical potential (μ_c) is able to provide variations in the charge carrier density in the radiation patch which in turn impacts the carrier mobility numbers and provides the graphene tunable. The specific details of the considered dielectric substrates with the implemented simulation and design procedure techniques are presented in Table 3.

With the use of the aforementioned specifications of the dielectric substrate and graphene patch dimensions, as well as their physical characteristics, the radiation performance of the plasmonic antennas is determined and discussed in the next section.

Table 2 Optimized plasmonic antenna dimensions (units in μm)	Parameter	W_p	L_p	W_f	L_f	G	W_g	L_g	h
	Values	35	28	9.15	13.5	1.5	55	48	5

Table 3 Simulation detailed information of recommended antenna

	Parameters	Value	Unit
Simulation solver	Time domain solver	FDTD	–
	Range frequency	1.0 to 5.0	THz
	Mesh type	Hexahedral	–
	Impedance	50	Ohm
Substrate	Types	SiO_3N_4	–
	Relative permittivity	9.5	–
	Loss tangent	0.0001	–
	Density	3290	kg/m^3
	Young's modulus	2.5×10^9	N/m^2

Results and Discussions

The radiation performances of the multiband plasmonic graphene patch antenna are investigated using different chemical potential (μ_c) by implementing CST at the operating frequency ranges from 0 to 5 THz. The characteristic of the multiband proposed antenna is analyzed in regard to reflection loss (S11), voltage standing wave ratio (VSWR), gain, efficiency, bandwidth (BW), fractional bandwidth (FBW), and far-field radiation pattern, as well as their E and H plane patterns.

Dual-Band Operation

The essential antenna characteristic is S11, and it could be lower than − 10 dB for suitable antenna impedance matching. Figures 3 and 4 display the proper operating frequency where S11 and VSWR parameters have minimum values with regard to the antenna bandwidth (BW). The change in the operating frequency (f_r) dependent on the μ_c is immediately apparent from the S11 and VSWR parameter curve.

This dependence indicates that the plasmonic antenna can be tuned within a frequency range, which shifts from 0.795 to 0.855 THz in the first excited vibration mode (TM10), while shifting from 3.605 to 3.790 THz in the second excited vibration mode (TM20) and from 4.647 to 4.670 THz in the third excited vibration mode at TM11. The plasmonic nano-antenna is simulated in the μ_c value which varies from 0.0 to 1.0 eV, which can be achieved simply through an external DC voltage source. Besides, for every chemical potential, the S11, VSWR, operating frequency, gain, efficiency, bandwidth (BW), and fractional bandwidth (FBW) of the
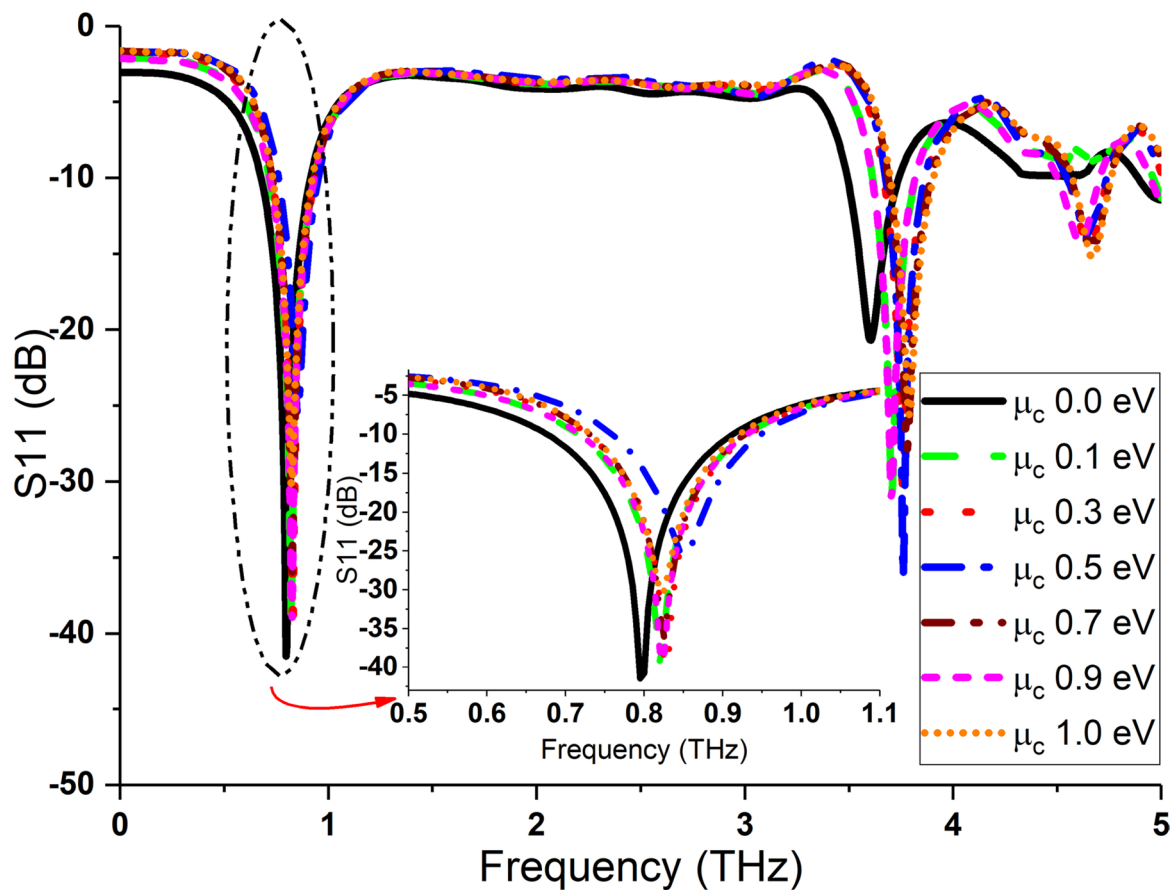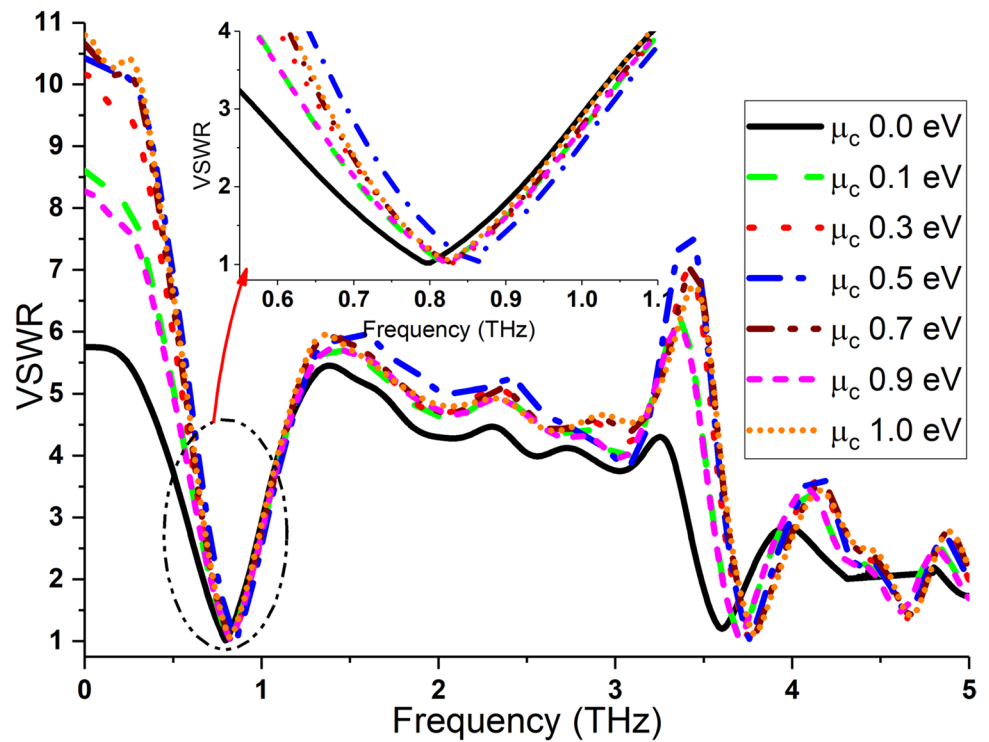

Fig. 3 Changing of S11 versus frequency of the plasmonic antenna with distinct μ_c

Fig. 4 Changing of VSWR versus frequency of the plasmonic antenna with distinct μ_c

proposed antenna are measured and the results are demonstrated in Table 4. It is clearly seen from this table that the minimum values of S11 and VSWR are −42.374 dB and 1.015, respectively, which are recorded at the μ_c value of 0.5 eV and at the resonance frequency of 0.855.

Moreover, the antennas with both μ_c of 0.0 and 0.1 eV are resonating at dual-band frequencies, which are 0.795 and 0.820 THz at the first excited mode (TM10) and 3.605 and 3.705 THz for the second excited mode (TM20) with S11 values of −41.484 and −39.559 and −20.683

Table 4 Plasmonic graphene-based patch antenna parameters for various chemical potential values

| μ_c (eV)	Band	f_r (THz)	BW (THz)	FBW (%)	S11 (dB)	VSWR	Gain (dB)
0.0	Dual band	0.795	0.248	31.32	−41.484	1.017	2.64
		3.605	0.262	7.24	−20.683	1.203	6.61
0.1	Dual band	0.820	0.243	29.63	−39.559	1.020	2.71
		3.705	0.224	6.05	−31.018	1.066	6.73
0.3	Tri-band	0.830	0.232	27.83	−39.955	1.021	2.83
		3.755	0.212	5.75	−30.263	1.063	7.43
		4.647	0.201	4.30	−14.715	1.450	6.56
0.5	Tri-band	0.855	0.202	32.40	−42.374	1.015	3.06
		3.760	0.202	5.21	−36.389	1.030	7.69
		4.650	0.196	4.24	−16.058	1.373	7.53
0.7	Tri-band	0.825	0.202	23.88	−36.046	1.032	2.97
		3.780	0.209	5.37	−27.927	1.083	7.29
		4.665	0.189	4.07	−14.936	1.436	6.53
0.9	Tri-band	0.825	0.222	26.91	−39.244	1.022	2.75
		3.705	0.209	5.67	−31.205	1.056	7.56
		4.605	0.202	4.41	−14.220	1.482	6.59
1.0	Tri-band	0.820	0.196	23.90	−30.173	1.063	2.71
		3.790	0.215	5.51	−25.025	1.110	7.21
		4.670	0.183	3.94	−15.253	1.417	6.66
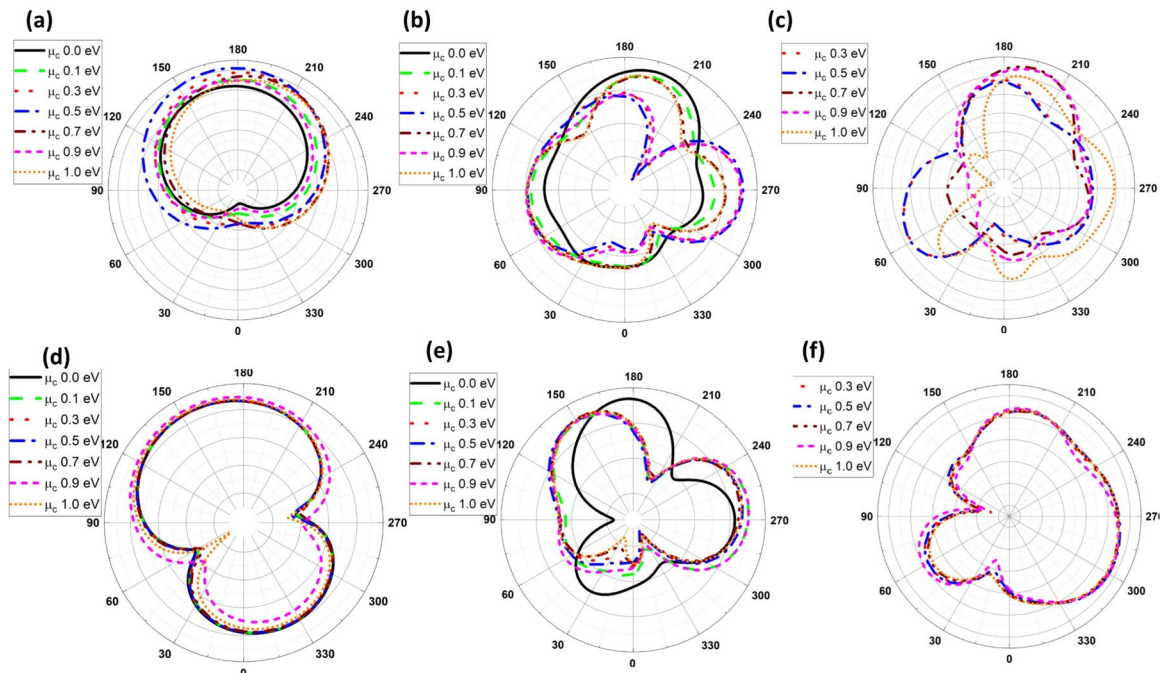
Fig. 5 2D representation of the recommended plasmonic graphene-based antenna radiation pattern for E plane **a** TM10, **b** TM20, and **c** TM11 and for H plane **d** TM10, **e** TM20, and **f** TM11 modes

and −31.018 dB, respectively. Besides, the implementation of other studied chemical potential values makes the proposed plasmonic antenna to operate at triple-band frequencies with acceptable values of S11 and VSWR. Furthermore, the wider fractional antenna bandwidth of 32.40% is also observed with the μ_c value of 0.5 eV for the first excited vibration modes (TM10). In addition, this table also displays that the second excited vibration modes (TM20) provide a higher antenna gain value of 7.69 dB with the use of all considered chemical potential

values. On the other side, the 2D view electric (E) and magnetic(H) planes of far-field radiation pattern for the first (TM10), second (TM20), and third excitation mode (TM11) of the plasmonic antenna for each chemical potentials are also measured and displayed in Fig. 5.

These figures demonstrate a directional E plane while a bidirectional H plane for the first excited vibration mode. However, in the second resonant modes, both E and H planes show a semi-omnidirectional pattern with some back and side lobes. Besides, the radiation figures for the
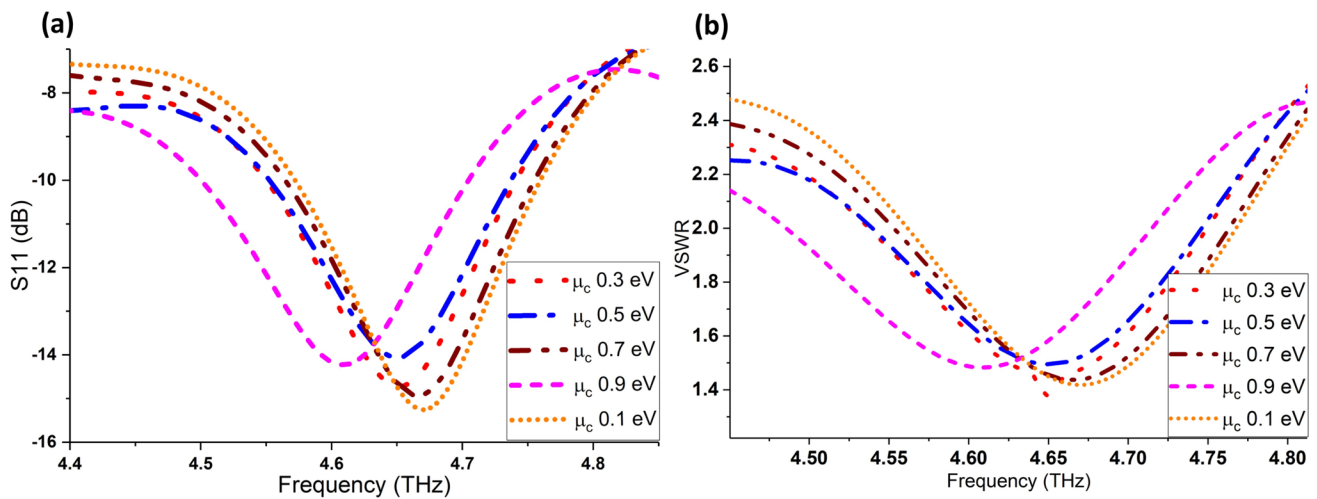

Fig. 6 The S11 and VSWR depended on frequency with various μ_c at TM11
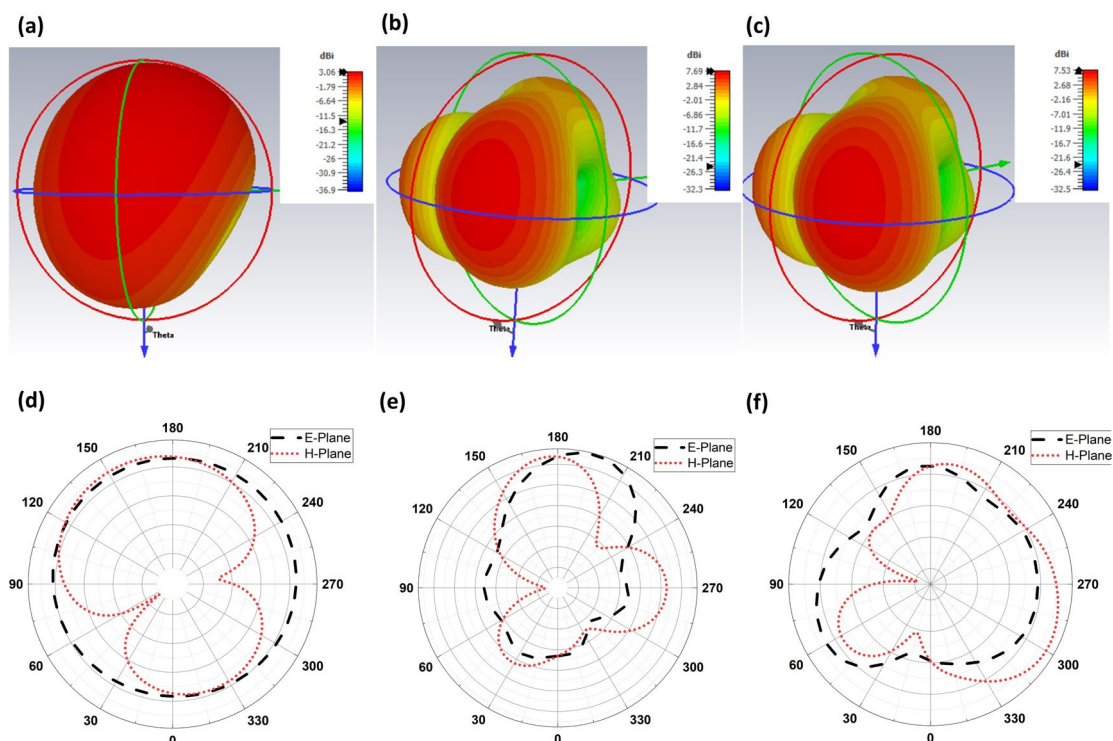
Fig. 7 3D view of the radiation far field at **a** 0.855 THz, **b** 3.760 THz, and **c** 4.650 THz and 2D view of the E plane and H plane at **d** 0.855 THz, **e** 3.760 THz, and **f** 4.650 THz for TM10, TM20, and TM11 mode with μ_c of 0.5 eV

third resonant frequencies display generally an approximate bidirectional E plane and H plane.

Change of μ_c for Tri-band Operation

In this section, the influence of μ_c on the antenna parameter printed on SiO_3N_4 as a dielectric substrate is investigated, which is widely employed in solar cell technologies. In addition, it can be supported multiband resonant that develop it suitable for designing new smart antennas. As explained by the results presented in Table 4, it is clear to see that the recommended antenna operates at a dual-band frequency at 0.795 and 3.605 THz and 0.820 and 3.705 THz, respectively, for the μ_c values of 0.0 and 0.1 eV. However, with an increase in μ_c from 0.3 to 1.0 eV, a third mode of vibration appears at frequencies 4.647, 4.650, 4.665, 4.605, and 4.670 THz, respectively. The excitation of the third vibration modes can be attributed to the fact that as the chemical potential increases fringe line fields will be produced along the edge of the antenna patch. Consequently, the stored energy in the plasmonic nano-antenna resonator reduces. Therefore, the antenna quality factor (Q_c) decreases, and thus, the antenna bandwidth (BW) of the proposed plasmonic antenna is changed.

As a result, the fundamental vibration mode is transvers magnetic mode (TM10) [49]. However, when the chemical potential becomes higher, sufficient carrier charge density is

formed within the antenna patch and this causes the antenna to operate with a high-order vibration mode, for example, TM10, TM20, and TM30, to propagate due to the creation of SPP at THz frequencies. The above modes will produce resonance equivalent to TM10 but in different frequency bands due to a different phase angle. Therefore, with the appropriate chemical potential values, the plasmonic patch antenna can be adjusted to resonate at tri-band frequencies.
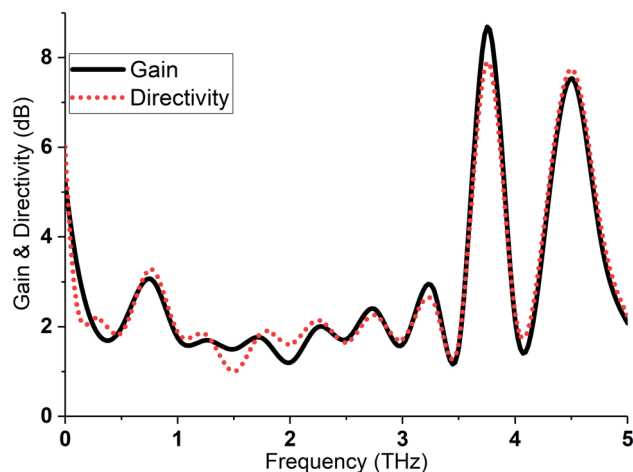

Fig. 8 Directivity and gain relative to frequency of the proposed plasmonic antenna with a μ_c value of 0.5 eV

Therefore, the total antenna radiation parameters that are summarized in Table 4 imply that the reliable chemical potential values of the graphene patch for tri-band operation appear to be at 0.3 eV and 0.5 eV. On the other hand, whenever μ_c is greater than the aforementioned limit, the ability of the presented plasmonic graphene patch antenna will be reduced due to the creation of surface waves. Generally, the advised plasmonic nano-antenna operates within a dual-band frequency as μ_c are below 0.1 eV, while beyond this value it resonates with a tri-band frequency. In addition, the variance of S11 and VSWR in tri-band operations is calculated again and the results are shown in Fig. 6. These two figures indicate that all considered chemical potential values provide acceptable S11 and VSWR values.

Furthermore, the 2D and 3D view of the radiation pattern for the tri-band antenna with μ_c of 0.5 eV is computed and the results are illustrated in Fig. 7. This figure demonstrates omnidirectional pattern behavior of the plasmonic nano-antenna in the first excited vibration mode at 0.855 THz, contrarily a bidirectional pattern for the second excited mode at 3.760 THz and an approximate bidirectional pattern for the third resonant mode at 4.650 THz.

Moreover, the directivity and realized gain for the advised plasmonic nano-antenna are also measured in the considered frequency bands and the achieved results are demonstrated in Fig. 8. This figure indicates that the recommended antenna resonated at triple-band frequencies of

Table 5 Tri-band plasmonic antenna compared to previously published work

Reference	Band	Substrate type	f_r (THz)	μ_c (eV)	BW (GHz)	Gain (dB)	Size (μm²)	Feeding method
[50]	Single band	Polyimide	0.51	0.18	400	5.49	600×300	TL-fed
[51]		Polyimide	2.96		797	5.40	60×60	TL-fed
[52]		Polyimide	1.90	0.50	–	4.50	120×90	TL-fed
[53]		–	2.02	1.00	–	8.91	256×216	CPW-fed
[54]		Al_2O_3	2.70	–	240	–	100×63	Edge-fed
[54]		Si_3N_4	2.70	–	270	–	100×63	Edge-fed
[6]	Dual band	FR4	3.50	0.40	400	1.46	120×95	Inset-fed
			4.33		460	2.34		
[55]		Al_2O_3	1.40	–	400	–	105×65	CPW-fed
			3.10		150	–		
[36]		GaAs	0.83	0.45	218	2.79	70×60	TL-fed
			3.67		178	3.03		
[56]		Polyamide	0.71	–	4.71	5.14	536×526	TL-fed
			0.74		3.13	5.00		
[57]		Silicon	2.48	0.25	115.1	2.70	65×65	TL-fed
			3.35		140.5	6.03		
[55]		Si_3N4	1.30	–	305	–	105×65	CPW-fed
			3.10		50	–		CPW-fed
Present work		**SiO_3N_4**	**0.82**	**0.50**	**243**	**2.71**	**55×48**	**Coupled gap-fed**
			3.70		**224**	**6.73**		
[6]	Tri-band	RT 5880	2.32	0.40	230	0.99	120×95	Inset-fed
			3.53		520	1.93		
			4.38		610	2.58		
[58]		Liquid crystalline polymer	0.10	–	1.80	15.82	360×590	TL-fed
			0.63		17.30	16.52		
			0.83		24.30	16.37		
[59]		SiO_2	1.95	0.3	–	4.79	50×50	Inset-fed
			4.83		–	5.05		
			5.44		–	5.53		
[36]		GaAs	0.77	0.45	203	2.51	70×60	TL-fed
			3.28		224	2.73		
			4.51		324	6.56		
Present work		**SiO_3N_4**	**0.85**	**0.50**	**202**	**3.06**	**55×48**	**Coupled gap-fed**
			3.76		**202**	**7.69**		
			4.65		**196**	**7.53**		

TL transmission line, *CPW* coplanar waveguide

0.855, 3.760, and 4.650 THz with a gain of 3.06, 7.65, and 7.53 dB, respectively.

Lastly, the calculated gain, bandwidth (BW), and size of the simulated tri-band antenna with the use of a μ_c value of 0.5 eV are compared to the earlier achieved by other research teams and the achievements are listed in Table 5. It is clearly seen from this table that the bandwidth, gain, and size of the proposed antennas agree with the recent available published works cited here at dual-band and tri-band operating frequencies. Additionally, the results have advantages of miniaturizing antenna size and operates with a higher gain and broad bandwidth (BW) values.

Conclusion

This article involves the design and analyses of a high-performance multiband plasmonic antenna. It is consists of graphene patch placed on the silicon nitride (SiO_3N_4) dielectric substrate to be used in terahertz wireless communication systems. The design procedure is performed by utilizing CST simulation technique and investigating different graphene chemical potential values in the range of 0.0 to 1.0 eV. Generally, the calculated results reveal that the operating frequency of the graphene patch antenna can be simply tuned through its chemical potential.

In addition, the simulation result implies that, as chemical potentials raised to more than 0.3 eV, the proposed antenna resonates with a triple-band frequency. Meanwhile, better values of gain are 3.06, 7.69, and 6.53 dB and fractional bandwidths are 32.4%, 5.21%, and 4.24% when μ_c is equal to 0.5 eV, at the frequencies of 0.766, 3.285, and 4.510 THz, respectively. On the other hand, the computed far-field radiation pattern displays an omnidirectional, a bidirectional, and an approximate bidirectional pattern behavior for the first, second, and third excited resonant modes, respectively. The reliability of the proposed antenna relies on multiband operating frequencies; it is smaller in size and provides high gain and a wider bandwidth compared to the corresponding values recently achieved by other researchers using another dielectric substrate with different feeding techniques. Therefore, it can be said that the proposed plasmonic antenna is suitable for high-speed indoor wireless application systems especially in the field of medical imaging, material identification, and security scanning in the terahertz frequency range.

Declarations

References

1. Saraereh OA, Al-Tarawneh L, Ali A, Hadidi A-MA (2022) Design and analysis of a novel antenna for THz wireless communication. Intell Autom Soft Comput 31(1):607–619. https://doi.org/10.32604/iasc.2022.020216
2. Mohammed SL, Alsharif MH, Gharghan SK, Khan I, Albreem M (2019) Robust hybrid beamforming scheme for millimeter-wave massive-MIMO 5G wireless networks. Symmetry 11(11):1424. https://doi.org/10.3390/sym11111424
3. Fakhte S, Taskhiri MM (2023) Graphene-enabled terahertz dielectric rod antenna with polarization reconfiguration. Opt Quant Electron 55(14):1258. https://doi.org/10.1007/s11082-023-05586-y
4. Sizov F, Rogalski A (2010) THz detectors. Prog Quantum Electron 34(5):278–347. https://doi.org/10.1016/j.pquantelec.2010.06.002
5. Qasem N, Marhoon HM (2020) Simulation and optimization of a tuneable rectangular microstrip patch antenna based on hybrid metal-graphene and FSS superstrate for fifth-generation applications. TELKOMNIKA (Telecommunication Computing Electronics and Control) 18(4):1719–1730. https://doi.org/10.12928/telkomnika.v18i4.14988
6. Khaleel SA, Hamad EKI, Saleh MB (2022) High-performance tri-band graphene plasmonic microstrip patch antenna using superstrate double-face metamaterial for THz communications. J Electr Eng 73(4):226–236. https://doi.org/10.2478/jee-2022-0031
7. Kavitha S, Sairam KVSSSS, Singh A (2022) Graphene plasmonic nano-antenna for terahertz communication. SN Appl Sci 4(4):114. https://doi.org/10.1007/s42452-022-04986-1
8. Jamshed MA, Nauman A, Abbasi MAB, Kim SW (2020) Antenna selection and designing for THz applications: suitability and performance evaluation: a survey. IEEE Access 8:113246–113261. https://doi.org/10.1109/ACCESS.2020.3002989
9. Krasikov S, Tranter A, Bogdanov A, Kivshar Y (2022) Intelligent metaphotonics empowered by machine learning. Opto-Electron Adv 5(3):210147. https://doi.org/10.29026/oea.2022.210147
10. Kiani N, Hamedani FT, Rezaei P (2023) Designing of a circularly polarized reconfigurable graphene-based THz patch antenna with cross-shaped slot. Opt Quant Electron 55(4):356. https://doi.org/10.1007/s11082-023-04617-y
11. Wu Y, Yu T, Shen Z (2010) Two-dimensional carbon nanostructures: fundamental properties, synthesis, characterization, and potential applications. J Appl Phys. https://doi.org/10.1063/1.3460809
12. Geim AK, Novoselov KS (2007) The rise of graphene. Nat Mater 6(3):183–191. https://doi.org/10.1038/nmat1849

13. Kiani N, Tavakol Hamedani F, Rezaei P (2022) Implementation of a reconfigurable miniaturized graphene-based SIW antenna for THz applications. Micro Nanostructures 169:207365. https://doi.org/10.1016/j.micrna.2022.207365

14. Chashmi MJ, Rezaei P, Kiani N (2019) Reconfigurable graphene-based V-shaped dipole antenna: from quasi-isotropic to directional radiation pattern. Optik 184:421–427. https://doi.org/10.1016/j.ijleo.2019.04.125

15. Fakharian M, Rezaei P, Orouji A (2015) Reconfigurable multi-band extended U-slot antenna with switchable polarization for wireless applications. IEEE Antennas Propag Mag 57(2):194–202. https://doi.org/10.1109/MAP.2015.2414665

16. Wang X, Zhi L, Müllen K (2008) Transparent, conductive graphene electrodes for dye-sensitized solar cells. Nano Lett 8(1):323–327. https://doi.org/10.1021/nl072838r

17. Shen LF, Xie JP, Wang ZH (2021) Tunable TM modes in a slab waveguide including a graphene-dielectric multilayer structure. Optik 227:165414. https://doi.org/10.1016/j.ijleo.2020.165414

18. Kiani N, Afsahi M (2019) Design and fabrication of a compact SIW diplexer in C-band. Iran J Electr Electron Eng 15(2):189

19. Deng Q et al (2019) Adjustable plasmonic multi-channel demultiplexer with graphene sheets and ring resonators. Plasmonics 14:993–998. https://doi.org/10.1007/s11468-018-0885-1

20. Jaiswal RK, Pandit N, Pathak NP (2019) Center frequency and bandwidth reconfigurable spoof surface plasmonic metamaterial band-pass filter. Plasmonics 14(6):1539–1546. https://doi.org/10.1007/s11468-019-00948-3

21. Bouanane I et al (2023) Design of infrared optical absorber using silver nanorings array made by a top-down process. Sci Rep 13(1):7770. https://doi.org/10.1038/s41598-023-34579-w

22. Vafapour Z et al (2021) The potential of refractive index nanobiosensing using a multi-band optically tuned perfect light metamaterial absorber. IEEE Sens J 21(12):13786–13793. https://doi.org/10.1109/JSEN.2021.3070731

23. Asgari S, Granpayeh N, Fabritius T (2020) Controllable terahertz cross-shaped three-dimensional graphene intrinsically chiral metastructure and its biosensing application. Opt Commun 474:126080. https://doi.org/10.1016/j.optcom.2020.126080

24. Eslami A, Sadeghi M, Adelpour Z (2021) Plasmonic modulator utilizing graphene-HfO2-ITO stack embedded in the silicon waveguide. Optik 227:165608. https://doi.org/10.1016/j.ijleo.2020.165608

25. Luan J et al (2019) Design and optimization of a graphene modulator based on hybrid plasmonic waveguide with double low-index slots. Plasmonics 14:133–138. https://doi.org/10.1007/s11468-018-0785-4

26. Fuscaldo W, Burghignoli P, Baccarelli P, Galli A (2017) Graphene Fabry-Perot cavity leaky-wave antennas: plasmonic versus non-plasmonic solutions. IEEE Trans Antennas Propag 65(4):1651–1660. https://doi.org/10.1109/TAP.2017.2670520

27. Nissiyah GJ, Madhan MG (2019) Graphene-based photoconductive antenna structures for directional terahertz emission. Plasmonics 14(4):891–900. https://doi.org/10.1007/s11468-018-0871-7

28. Zhu B, Ren G, Gao Y, Wu B, Lian Y, Jian S (2017) Creation of graphene plasmons vortex via cross shape nanoantennas under linearly polarized incidence. Plasmonics 12(3):863–868. https://doi.org/10.1007/s11468-016-0336-9

29. Fakhte S, Taskhiri MM (2023) Graphene-based terahertz antenna with polarization reconfiguration. Phys Scr 98(11):115541. https://doi.org/10.1088/1402-4896/ad03ca

30. Ameri A, Moradi G (2023) Reconfigurable graphene square patch antenna. Optik 284:170961. https://doi.org/10.1016/j.ijleo.2023.170961

31. Giddens H, Yang L, Tian J, Hao Y (2018) Mid-infrared reflectarray antenna with beam switching enabled by continuous graphene layer. IEEE Photonics Technol Lett 30(8):748–751. https://doi.org/10.1109/LPT.2018.2814684

32. Ekşioğlu Y, Cetin AE, Durmaz H (2018) Multi-band plasmonic platform utilizing UT-shaped graphene antenna arrays. Plasmonics 13(3):1081–1088. https://doi.org/10.1007/s11468-017-0607-0

33. Aditya RANS, Thampy AS (2019) Behavioral and modal analysis of graphene-based polygonal optical antenna for enhanced biomolecular detection. Plasmonics 14(2):293–302. https://doi.org/10.1007/s11468-018-0804-5

34. Hanson GW (2008) Dyadic Green's functions for an anisotropic, non-local model of biased graphene. IEEE Trans Antennas Propag 56(3):747–757. https://doi.org/10.1109/TAP.2008.917005

35. Zhao T, Hu M, Zhong R, Gong S, Zhang C, Liu S (2017) Cherenkov terahertz radiation from graphene surface plasmon polaritons excited by an electron beam. Appl Phys Lett. https://doi.org/10.1063/1.4984961

36. Ezzulddin SK, Hasan SO, Ameen MM (2023) Performance analysis of plasmonic nano-antenna based on graphene with different dielectric substrate materials for optoelectronics application. Plasmonics. https://doi.org/10.1007/s11468-023-02030-5

37. Hanson GW (2008) Dyadic Green's functions and guided surface waves for a surface conductivity model of graphene. J Appl Phys. https://doi.org/10.1063/1.2891452

38. Gusynin VP, Sharapov SG, Carbotte JP (2007) Magneto-optical conductivity in graphene. J Phys Condens Matter 19(2):026222. https://doi.org/10.1088/0953-8984/19/2/026222

39. Aloui R, Houaneb Z, Zairi H (2019) Substrate integrated waveguide circular antenna for terahertz application. Prog Electromagn Res C 96:229–242. https://doi.org/10.2528/PIERC19080607

40. Kiani N, Tavakkol Hamedani F, Rezaei P (2023) Reconfigurable graphene-gold-based microstrip patch antenna: RHCP to LHCP. Micro Nanostructures 175:207509. https://doi.org/10.1016/j.micrna.2023.207509

41. Qin X, Chen J, Xie C, Xu N, Shi J (2016) A tunable THz dipole antenna based on graphene. In 2016 IEEE MTT-S International Microwave Workshop Series on Advanced Materials and Processes for RF and THz Applications (IMWS-AMP): IEEE, pp 1–3. https://doi.org/10.1109/IMWS-AMP.2016.7588365

42. Ameri A, Moradi G, Sarraf Shirazi R (2023) Reconfigurable graphene elliptic patch antenna. Opt Continuum 2(5):1148–1157. https://doi.org/10.1364/OPTCON.487974

43. Dash S, Patnaik A (2020) Behavior of graphene based planar antenna at microwave and terahertz frequency. Photonics Nanostruct Fundam Appl 40:100800. https://doi.org/10.1016/j.photonics.2020.100800

44. Ezzulddin SK, Hasan SO, Ameen MM (2022) Microstrip patch antenna design, simulation and fabrication for 5G applications. Simul Model Pract Theory 116:102497. https://doi.org/10.1016/j.simpat.2022.102497

45. Abbasi QH, Alomainy A, Jornet JM, Han C, Chen Y (2018) IEEE Access special section editorial: nano-antennas, nano-transceivers and nano-networks/communications. IEEE Access 6:8270–8272. https://doi.org/10.1109/ACCESS.2018.2805578

46. Kumar MR (2019) A compact graphene based nano-antenna for communication in nano-network. J Inst Electron Comp 1(1):17–27. https://doi.org/10.33969/JIEC.2019.11003

47. Correas-Serrano D, Gomez-Diaz JS, Perruisseau-Carrier J, Alvarez-Melcon A (2014) Graphene-based plasmonic tunable low-pass filters in the terahertz band. IEEE Trans Nanotechnol 13(6):1145–1153. https://doi.org/10.1109/TNANO.2014.2344973

48. Kushwaha RK, Karuppanan P, Malviya LD (2018) Design and analysis of novel microstrip patch antenna on photonic crystal in THz. Physica B 545:107–112. https://doi.org/10.1016/j.physb.2018.05.045

49. Jafari Chashmi M, Rezaei P, Kiani N (2020) Polarization controlling of multi resonant graphene-based microstrip antenna. Plasmonics 15(2):417–426. https://doi.org/10.1007/s11468-019-01044-2

50. Babu KV, Das S, Sree GNJ, Madhav BTP, Patel SKK, Parmar J (2022) Design and optimization of micro-sized wideband fractal

MIMO antenna based on characteristic analysis of graphene for terahertz applications. Opt Quant Electron 54(5):281. https://doi.org/10.1007/s11082-022-03671-2

51. Shamim SM et al (2023) Design and analysis of microstrip patch antenna with photonic band gap (PBG) structure for high-speed THz application. Opt Quant Electron 55(7):618. https://doi.org/10.1007/s11082-023-04834-5

52. Khaleel SA, Hamad EKI, Parchin NO, Saleh MB (2023) Programmable beam-steering capabilities based on graphene plasmonic THz MIMO antenna via reconfigurable intelligent surfaces (RIS) for IoT applications. Electronics 12(1):164. https://doi.org/10.3390/electronics12010164

53. Basiri R, Zareian-Jahromi E, Aghazade-Tehrani M (2022) A reconfigurable beam sweeping patch antenna utilizing parasitic graphene elements for terahertz applications. Photonics Nanostruct Fundam Appl 51:101044. https://doi.org/10.1016/j.photonics.2022.101044

54. Bala R, Marwaha A (2016) Investigation of graphene based miniaturized terahertz antenna for novel substrate materials. Eng Sci Technol Int J 19(1):531–537. https://doi.org/10.1016/j.jestch.2015.08.004

55. Sharma P, Yadav K, Bhattacharya PP (2020) Design of a graphene based miniaturized CPW fed antenna for terahertz applications. Int J Adv Microw Technol 5(4):242–246. https://doi.org/10.32452/IJAMT.2020.242246

56. Shihzad W, Ullah S, Ahmad A, Abbasi NA, Choi D-Y (2022) Design and analysis of dual-band high-gain THz antenna array for THz space applications. Appl Sci 12(18):9231. https://doi.org/10.3390/app12189231

57. Shalini M, Madhan MG (2019) Design and analysis of a dual-polarized graphene based microstrip patch antenna for terahertz applications. Optik 194:163050. https://doi.org/10.1016/j.ijleo.2019.163050

58. Rabbani MS, Ghafouri-Shiraz H (2017) Liquid crystalline polymer substrate-based THz microstrip antenna arrays for medical applications. IEEE Antennas Wirel Propag Lett 16:1533–1536. https://doi.org/10.1109/LAWP.2017.2647825

59. Shalini M, Madhan MG (2020) Performance predictions of slotted graphene patch antenna for multi-band operation in terahertz regime. Optik 204:164223. https://doi.org/10.1016/j.ijleo.2020.164223